α-Amino-β-carboxymuconic-ε-semialdehyde Decarboxylase (ACMSD) Is a New Member of the Amidohydrolase Superfamily†

Tingfeng Li,‡ Hiroaki Iwaki,§ Rong Fu,‡ Yoshie Hasegawa,§ Hong Zhang,|| and Aimin Liu*,‡

Department of Biochemistry, University of Mississippi Medical Center, Jackson, Mississippi 39216, Department of Biotechnology, Faculty of Engineering, Kansai University, Suita, Osaka 564-8680, Japan, and Department of Biochemistry, University of Texas Southwestern Medical Center, Dallas, Texas 75390

Received January 18, 2006; Revised Manuscript Received March 28, 2006

ABSTRACT: The enzymatic activity of *Pseudomonas fluorescens* α-amino-β-carboxymuconic-ε-semialdehyde decarboxylase (ACMSD) is critically dependent on a transition metal ion [Li, T., Walker, A. L., Iwaki, H., Hasegawa, Y., and Liu, A. (2005) *J. Am. Chem. Soc. 127*, 12282−12290]. Sequence analysis in this study further suggests that ACMSD belongs to the amidohydrolase superfamily, whose structurally characterized members comprise a catalytically essential metal cofactor. To identify ACMSD's metal ligands and assess their functions in catalysis, a site-directed mutagenesis analysis was conducted. Alteration of His-9, His-177, and Asp-294 resulted in a dramatic loss of enzyme activity, substantial reduction of the metal-binding ability, and an altered metallocenter electronic structure. Thus, these residues are confirmed to be the endogenous metal ligands. His-11 is implicated in metal binding because of the strictly conserved HxH motif with His-9. Mutations at the 228 site yielded nearly inactive enzyme variants H228A and H228E. The two His-228 mutant proteins, however, exhibited full metal-binding ability and a metal center similar to that of the wild-type enzyme as shown by EPR spectroscopy. Kinetic analysis on the mutants indicates that His-228 is a critical catalytic residue along with the metal cofactor. Since the identified metal ligands and His-228 are present in all known ACMSD sequences, it is likely that ACMSD proteins from other organisms contain the same cofactor and share similar catalytic mechanisms. ACMSD is therefore the first characterized member in the amidohydrolase superfamily that represents a C−C breaking activity.

The enzyme α-amino-β-carboxymuconic-ε-semialdehyde decarboxylase (ACMSD)[1] plays a key role in two natural metabolic events, i.e., 2-nitrobenzoic acid biodegradation in bacteria and L-tryptophan catabolism in mammals (*1*). As illustrated in Figure 1, this decarboxylase enzyme competes with a spontaneous reaction that leads to nicotinamide adenine dinucleotide (NAD) biosynthesis. The activity of ACMSD essentially determines the final fate of the metabolites in either pathway.

In the absence of ACMSD, ACMS is transformed to quinolinic acid (QUIN). QUIN is not only the precursor for NAD biosynthesis but also an excitotoxin (*2*−*6*). Elevated QUIN concentrations in body fluids are observed in an exceptionally wide range of neuropsychiatric disease states, including anxiety, depression, and epilepsy as well as neurodegenerative diseases such as Alzheimer's and Huntington's diseases (*3*, *6*). Since ACMSD competes with the spontaneous QUIN-forming reaction, activation of this enzyme may direct the metabolic flux to the citric acid cycle and thus produce a rapid response for pharmacological treatments of the above-mentioned psychosis and cognitive symptoms. Conversely, it may be imperative to inhibit ACMSD so that ACMS can undergo the spontaneous process to synthesize QUIN and NAD under vitamin B_6-deficient conditions (*7*, *8*). In animals with certain endocrine disturbances, particularly diabetes, there is a great increase in the concentration and activity of liver ACMSD (*9*). In this case, inhibition of ACMSD may help to alleviate the symptoms of these disturbances. Therefore, ACMSD has been recognized as an emerging drug target (*9*, *10*).

A special aspect of ACMSD concerns the catalytic cofactor in this enzyme. This decarboxylase has been studied for 5 decades since it was first isolated in 1956 (*7*, *9*, *11*−*16*). For a long period of time, ACMSD was thought to have no cofactor and may represent a new protein fold (*14*, *16*). Very recently, a pentacoordinate mononuclear metallocofactor has been uncovered in the first spectroscopic study of ACMSD from *Pseudomonas fluorescens* (*Pf*) (*1*). Several divalent metal ions, including Co(II) and Fe(II), can be taken up by

† This work was supported in part by funds from a subaward of NIH Grant GM069618 and American Cancer Society UMMC Intramural Grant 53439 (to A.L.), NIH Grant GM65243 (to H.Z.), and Mext. Haiteku (2002-2006) (to Y.H.).

* Corresponding author. Phone: 601-984-1872. Fax: 601-984-1501. E-mail: aliu@biochem.umsmed.edu.

‡ University of Mississippi Medical Center.

§ Kansai University.

|| University of Texas Southwestern Medical Center at Dallas.

[1] Abbreviations: ACMS, α-amino-β-carboxymuconic-ε-semialdehyde (or 2-amino-3-carboxymuconate-6-semialdehyde); ACMSD, α-amino-β-carboxymuconic-ε-semialdehyde decarboxylase (EC 4.1.1.45, previously known as picolinic acid carboxylase); 2-AMS, 2-aminomuconate-6-semialdehyde; EPR, electron paramagnetic resonance spectroscopy; 3-HAA, 3-hydroxyanthranilic acid; IDCase, isoorotate decarboxylase (EC 4.1.1.66, also known as uracil-5-carboxylate decarboxylase); 2-NBA, 2-nitrobenzoic acid; *Pf*, *Pseudomonas fluorescens*; QUIN, quinolinic acid.

10.1021/bi060108c CCC: $33.50
Published on Web 05/09/2006

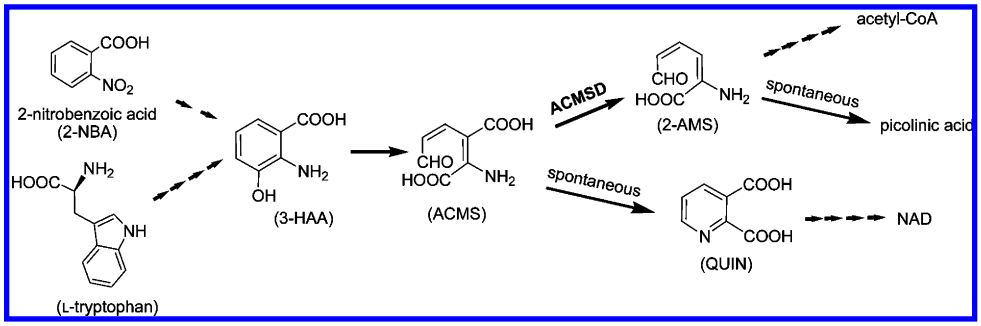

FIGURE 1: The enzyme ACMSD controls the flow of metabolic intermediates to either acetyl-CoA or NAD/NADP in both 2-nitrobenzoic acid biodegradation and L-tryptophan's kynurenine catabolic pathways.

the enzyme in either cell growth or cell-free conditions to activate the specified decarboxylation activity. The Co(II)-containing enzyme has been shown to possess the highest specific activity under standard assay conditions. Furthermore, the reaction is shown to be oxidant-independent and proceeds in a nonoxidative fashion, demonstrating a novel, metal-dependent, oxidant-independent, biological decarboxylation (*1*).

Two important questions have risen from the finding of a metallocofactor in the *Pf* ACMSD. The first is the chemical nature of the cofactor. Despite quite distinct specific activities with different metal ions, the k_{cat}/K_m obtained are in the same range, implying that the metal cofactor functions as a Lewis acid catalyst rather than a redox center (*1*). To decipher whether the metal ion is a protein-bound cofactor, molecular characterization on ACMSD is required to identify the metal ligands. Second, it is not clear whether other ACMSD enzymes, especially those from the eukaryotic organisms involved in tryptophan catabolism, also contain a metallocofactor. If the metal ligands are identified from one ACMSD protein, the presence of the metallocofactor in the enzyme from other organisms can then be reliably predicted from sequence alignments.

In the present study, a comprehensive protein sequence analysis indicates a strong link between ACMSD and the metal-dependent amidohydrolase protein superfamily. A site-directed mutagenesis analysis is followed to experimentally assess the protein family categorization and identify protein ligands. The results described here reveal for the first time detailed information on the ACMSD catalytic center and eventually suggest that ACMSD is a prototypic member for an emerging subset of decarboxylase enzymes in the amidohydrolase superfamily.

EXPERIMENTAL PROCEDURES

Construction of Pseudomonas fluorescens ACMSD Expression Plasmids. Standard methods were used for DNA manipulations. Construction of wild-type nontagged ACMSD encoded by the *nbaD* gene of *P. fluorescens* in *Escherichia coli* has been described previously (*16*). In this work, an expression system of His_{10}-tagged ACMSD was constructed to facilitate the site-directed mutagenesis analysis of the enzyme active site. The *nbaD* gene encoding *Pf* ACMSD was amplified by PCR with forward primer 5′-GGA ATT CCA TAT GAA AAA ACC GCG GAT TGA TA-3′ and reverse primer 5′-CCC TCG AGA CCA TTA AAC ATT GAT ATT G-3′. The PCR product was purified from 0.8% agarose gel, digested with *Nde*I and *Xho*I, and ligated into the equivalent sites of pET16b.

Mutagenesis of Pf ACMSD. The plasmid containing His_{10}-tagged ACMSD was used as a template for construction of all of the mutants. ACMSD single mutants except H9E were constructed by the PCR overlap extension mutagenesis technique (*17*). The following forward primers were used for construction of site-directed ACMSD mutants of H177A, H228A, H228E, and D294E: H177A-F, 5′-ATA TTC CAA TCT TGG TTG CCC CAT GGG ACA TGA TG-3′; H228A-F, 5′-CAA GAT CTG TTT CGG GGC GGG TGG GGG AAG TTT CG-3′; H228E-F, 5′-CAA GAT CTG TTT CGG GGA AGG TGG GGG AAG TTT CG-3′; and D294E-F, 5′-TGA TGC TTG GAT CGG AAT ACC CGT TCC CGC TGG-3′. The reverse primers used for the creation of the above mutants were the complement of the forward primers. H9E was constructed by PCR using the mutagenic primer 5′-GGA ATT CCA TAT GAA AAA ACC GCG GAT TGA TAT GGA ATC GCA CTT CTT CCC CC-3′ and T7 terminator primer. The insert for each of the above constructs was verified by DNA sequencing to ensure that base changes had been introduced correctly and no random change had occurred. After sequencing, the positive clone was used for high-level expression in *E. coli* BL21(DE3) by isopropyl β-D-thiogalactopyranoside (IPTG) induction.

Bacterial Growth with Supplemented Metal Salts. E. coli strains BL21(DE3) encoding native and His_{10}-tagged ACMSD (wild-type and mutants) plasmids were inoculated into autoclaved LB medium containing 100 μg/mL ampicillin and cultured at 37 °C. For ACMSD induction, IPTG was added to a final concentration of 0.5 mM at ca. 0.6 OD at 600 nm. The culture was allowed to grow continuously for an additional 4 h at 28 °C before harvesting.

Protein Preparations. The frozen cells containing overexpressed ACMSD or site-directed mutants were resuspended in a 50 mM potassium phosphate buffer, pH 8.0, containing 10 mM β-mercaptoethanol and 0.1 mg/mL lysozyme. The cell slurry was sonicated, and the debris was removed by centrifugation at 27000*g* for 30 min at 4 °C. The cell-free extract of histidine-tagged ACMSD was purified by either Ni-NTA superflow (Qiagen) resin or prepacked HisPrep FF columns (GE Healthcare) using an ÄKTA FPLC protein purification system. The major fractions with ACMSD activity were pooled, concentrated, and desalted by gel filtration on a HiPrep 26/10 desalting column (GE Healthcare). For apoprotein preparations, the pool was mixed with 5 mM EDTA for overnight with gentle shaking in a cold room before the gel filtration process. This process ensured that any metal ions from the metal-affinity resin were stripped off from ACMSD proteins. The protein concentration was determined by using Coomassie Plus protein assay reagent

(Pierce) according to the manufacturer's protocol. The expression level and enzyme purity were determined by SDS−PAGE on 12% polyacrylamide gels.

Preparation of ACMS. A stock solution (0.4 M) of 3-hydroxyanthranilic acid was freshly prepared in DMSO. It was diluted 100 times with O_2-saturated 25 mM HEPES, pH 7.0, and 5% glycerol before mixing with 3-hydroxyanthranilate 3,4-dioxygenase, which contained no free transient metal ion. ACMS production was monitored by measuring absorbance at 360 nm ($\epsilon_{360nm} = 47500\ M^{-1}\ cm^{-1}$) (*18*).

Steady-State Kinetic Analysis of ACMSD Mutants. Specific activities of the wild-type and variant ACMSD proteins were determined aerobically by a spectrophotometric assay on an Agilent 8453 diode-array spectrophotometer. When the substrate concentration was equal to or lower than 25 μM, absorbance at 360 nm was used to calculate the reaction rates. Due to the high extension coefficient of ACMS, the absorption maximum at 360 nm was not suitable to measure for determination of rate constants with most of the mutant experiments since greater than 25 μM substrate concentrations were required. In the latter case, absorbance at 320 nm was used to measure rate constants. The steady-state experiments were conducted at 22 ± 1 °C in 25 mM HEPES buffer, pH 7.0, containing 5% glycerol. Initial velocities were calculated from the raw data subtracted from those of control reaction mixtures in the absence of ACMSD. Kinetic constants were determined from the Lineweaver−Burk double reciprocal plots.

Reconstitution of Apoprotein with Metal Ions. Apo ACMSD and mutants were reconstituted with one equivalent amount of $CoCl_2$ from a freshly prepared stock solution. Reconstituted wild-type ACMSD had an activity of 6000 nmol min^{-1} mg^{-1} in HEPES buffer, pH 7.0. The metal-recharged ACMSD was either added to a freshly generated ACMS solution for enzyme assay or transferred to a quartz tube for EPR measurements.

Structure-Based Sequence Alignment. The sequence of *Pf* ACMSD (g_i 28971629) was used as a query to search the NCBI Conserved Domain Database with rpsblast (*19*), the Pfam database (*20*), and NCBI nonredundant protein sequence database with PSI-BLAST (*21*). The sequences of ACMSD homologues obtained from the PSI-BLAST search were aligned using program PCMA (*22*). Secondary structure prediction for ACMSD was performed with the PSIPRED protein structure prediction server (*23*).

Spectroscopic Analysis. UV−vis spectra were obtained in 25 mM HEPES buffer, pH 7.0, and 5% glycerol at 22 °C. X-band EPR spectra were obtained at 10 K on a Bruker EMX spectrometer. HEPES buffer (25 mM, pH 7.0) containing 5−10% glycerol was used in the EPR sample preparations. Spin quantitation was performed by comparing the double integration using the wild-type enzyme as a standard to determine the relative metal contents in the point mutants. EPR simulation was conducted as described previously (*1*).

RESULTS

Sequence Analysis Suggests That ACMSD Belongs to a Large Metal-Dependent Hydrolase Superfamily. ACMSD has been purified from cat, hog, rat, human, *Caenorhabditis elegans*, and *P. fluorescens*, and the enzymatic decarboxylation activities have been demonstrated in the corresponding proteins (*7*, *10*−*15*, *24*, *25*). Previously, 16 complete protein sequences in GenBank and NCBI databases were annotated as ACMSD or hypothetical ACMSD proteins. Alignment of all 16 ACMSD protein sequences by ClustalW indicated 34 highly conserved residues, and it offered little help for identifying metal-binding motifs (not shown). The putative ACMSD sequences are growing rapidly in the protein databases. We then used the *Pf* ACMSD (g_i 28971629) sequence as a query to search various protein databases and found that ACMSD comprises the protein family COG2159 in the COGs database (*26*) and PF04909 in the Pfam database (*20*). Both databases predict that ACMSD is related to a large metal-dependent hydrolase superfamily that includes urease, adenosine deaminase, phosphotriesterase, and dihydroorotase, among others (*27*). Many members of this superfamily are well characterized functionally and structurally (*28*). Enzymes in this superfamily adopt the $(\beta/\alpha)_8$-barrel fold with eight strands of parallel β-sheet flanked on the outside with α-helices (known also as TIM-barrel fold) (*28*). The active site of the enzymes in this superfamily contains either a binuclear or mononuclear metal center, which is catalytically essential. Protein residues that function as metal ligands typically include an HxH metal-binding motif at the end of the first β strand, one histidine at the end of the fifth β-strand, one histidine at β-strand 6, and an aspartic acid from the end of the eighth β-strand (Figure 2).

A multiple sequence alignment of ACMSD from various species along with eight representative members of the amidohydrolase superfamily was created using the program PCMA (*22*). This alignment reveals that all of the typical metal ligands are conserved in ACMSD (Figure 2). In *Pf* ACMSD, the first two histidine residues (HXH) at the end of the first β-strand are His-9 and His-11. For a mononuclear metal cofactor, the third histidine ligand is typically contributed by the β5 or β6 strand. His-177 and His-228 are the apparent candidates in *Pf* ACMSD (Figure 2). A carboxylate ligand is often donated by the β8 strand, and the invariant Asp-294 is in position to fulfill this role (Figure 2). There are no conserved glutamate or lysine residues in the ACMSD sequences in the putative β3 and β4 strands that can function as a bridging ligand for a binuclear metal center.

Functional Analysis of the ACMSD Mutants. Site-directed mutants H9E, H177A, H228A, H228E, and D294E of *Pf* ACMSD were constructed and expressed as soluble proteins. Since His-9 and His-11 are located at the same β-strand and they both are anticipated metal ligands, we chose His-9 as a mutational target to examine the role of the HxH motif. All ACMSD mutants were expressed at a very high level comparable to that of the wild-type enzyme as judged by SDS−PAGE (data not shown), indicating that the mutations had not affected the overall folding of the protein. Alteration of the putative metal ligand residues, His-9, His-177, His-228, and Asp-294, significantly lowered the enzyme activity. Table 1 summarizes kinetic properties of the enzyme variants. The k_{cat}/K_m numbers determined for the mutants are at least one magnitude lower than that of the wild-type enzyme, indicating a significantly reduced catalytic efficiency of the mutants. Replacement of histidine to alanine at the 177 and 228 sites resulted in a small decrease of K_m in both mutant proteins than that of wild type and His-9 as well as Asp-294 mutants. In fact, D294E exhibited a small, but noticeable

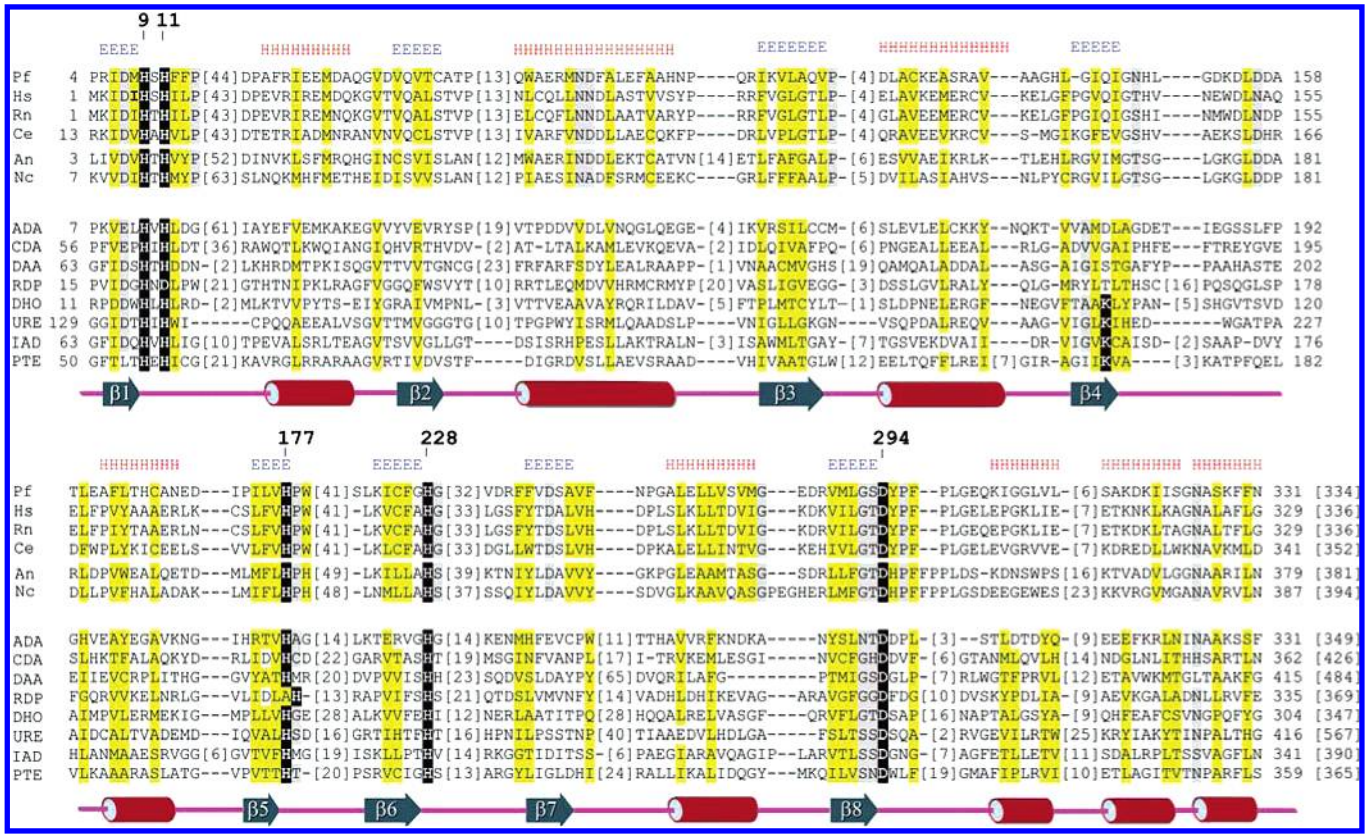

FIGURE 2: Multiple sequence alignment of representative sequences of ACMSD (first four sequences in the upper block), IDCase (last two sequences in the upper block), and representative members of the amidohydrolase superfamily with known structures (lower block). The first and last residue numbers are indicated before and after each sequence with the lengths of insertions specified in parentheses and the total sequence length of each protein following in square brackets. The invariant active site residues including metal ligands are indicated and highlighted in black. Conserved small residues are highlighted in gray. Uncharged residues in mainly hydrophobic sites are highlighted in light yellow. Predicted ACMSD α-helices (H) and β-strands (E) are labeled at the top of the alignment. General locations of the secondary structure elements are marked below the alignment. The sequences included in the alignment are ACMSD from *P. fluorescens* (Pf, g_i 28971629), *Homo sapiens* (Hs, g_i 37999723), *Rattus norvegicus* (Rn, g_i 18652911), and *Caenorhabditis elegans* (Ce, g_i 15150701) as well as IDCase from *Aspergillus nidulans* (An, g_i 67515537) and *Neurospora crassa* (Nc, g_i 51872137). Selected amidohydrolase enzymes with known structures are as follows: ADA, mouse adenosine deaminase (PDB code 1a4m) (*36*); CDA, *E. coli* cytosine deaminase (1k6w) (*43*); DAA, D-aminoacylase from *Alcaligenes faecalis* (1m7j) (*44*); RDP, human renal dipeptidase (1itu) (*45*); DHO, *E. coli* dihydroorotase (1j79) (*35*); URE, the C subunit of *Klebsiella aerogenes* urease (1fwb) (*46*); IAD, *E. coli* isoaspartyl dipeptidase (1onw) (*47*); PTE, *Pseudomonas diminuta* phosphotriesterase (1psc) (*48*).

Table 1: Kinetic Properties of ACMSD Mutants[a]

ACMSD	K_m (μM ACMS)	k_{cat} (s^{-1})	k_{cat}/K_m ($s^{-1}\,M^{-1}$)
wild type	16.7 ± 0.1	6.65 ± 0.1	$(4.0 \pm 0.1) \times 10^5$
H9E	24.1 ± 4.0	0.025 ± 0.007	$(1.0 \pm 0.1) \times 10^3$
H177A	12.3 ± 4.0	0.28 ± 0.05	$(2.3 \pm 0.5) \times 10^4$
D294E	67.2 ± 24.1[b]	0.08 ± 0.03	$(1.2 \pm 0.7) \times 10^3$
H228A	7.5 ± 2.7	0.11 ± 0.12	$(1.5 \pm 0.\ 6) \times 10^4$
H228E	66.2 ± 12.1	0.019 ± 0.004	$(2.9 \pm 0.6) \times 10^2$

[a] See text for experimental conditions. [b] D294E was less stable compared to the wild-type enzyme and other site-directed mutants. This was the major reason for a relatively large standard deviation.

increase (ca. 4-fold) of K_m value as the consequence of replacement of the putative carboxylate ligand with a longer chain residue, i.e., glutamic acid over aspartic acid. The slightly increased K_m value was also observed in H228E. However, this change is likely due to a different mechanism, i.e., the negative charge introduced to the active site in the histidine-to-glutamic acid mutation. Nevertheless, the K_m values of the mutants are not significantly different from that of the wild-type enzyme, indicating that limited effects on the substrate binding were introduced by mutations.

Characterization of ACMSD Mutants by EPR Spectroscopy. Figure 3 shows representative EPR spectra obtained at 10 K. A very broad high-spin ($S = {}^3/_2$) cobalt(II) EPR signal has been characterized in the wild-type enzyme (*1*). In the present work, the EPR signal was used as a benchmark to examine the metal affinity and structure in the Co(II)-reconstituted mutants. Among the reconstituted proteins, His-228 mutants exhibited a high-spin ($S = {}^3/_2$) Co(II) center in the EPR spectrum which is remarkably similar to the wild-type enzyme with only a 2 mT shift to lower field of the g_x component, suggesting rather limited changes of the metal center's electronic structure by mutation of the 228 residue. In contrast, the EPR spectrum of D294E presented a high-spin Co(II) center with a much increased g-anisotropy and principal g values of 1.99, 4.26, and 4.61. The hyperfine coupling constant in the $g_\perp$ region, obtained from spectral simulation, was 387 MHz for the D294E mutant. The EPR data also reveal the low metal occupancy in His-9, His-177, and Asp-294. In this set of experiments, metal ions in ACMSD were stripped by vigorous 5 mM EDTA treatment from proteins. A gel-filtration process was followed to remove EDTA and any unbound inorganic complexes. The apo-ACMSD proteins were reconstituted with excessive $CoCl_2$ followed with a second chromatography desalting step to remove unbound metal ions. The Co(II)-recharged AC-

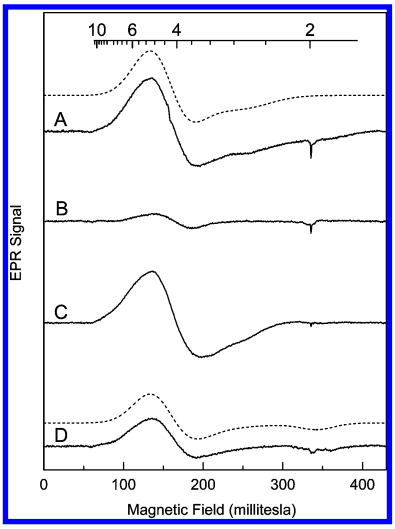

FIGURE 3: X-band 10 K EPR spectra of the cobalt(II)-containing ACMSD and representative mutants: (A) wild-type *Pf* ACMSD, (B) H177A, (C) H228A, and (D) D294E. The protein concentration was 0.3 mM except for H228A, which was 0.44 mM. Dotted traces are spectral simulations. Spectrometer conditions: temperature, 10 K; modulation amplitude, 0.3 mT; microwave power, 0.5 mW; time constant, 40.96 ms; sweep time, 5.96 mT/s for the entire field between 0.1 and 500 mT.

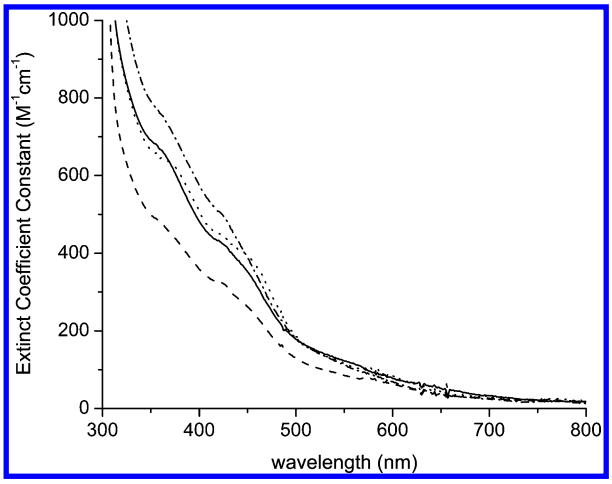

FIGURE 4: UV−vis spectra of ACMSD and selected mutants isolated from the cell culture supplemented with 0.5 mM $CoCl_2$. Protein concentrations: wild-type ACMSD, 0.46 mM (solid trace); H177A, 1.38 mM (dashed trace); H228A, 0.7 mM (dotted line); H228E, 0.44 mM (dash-dotted trace).

MSD proteins were examined by low-temperature EPR spectroscopy. The spin quantitation analysis revealed that H9E typically had a 0.12−0.15:1 metal-to-protein ratio. The variation of metal contents was due to the stripping and chromatography efficiencies as well as the low metal ion binding capacity of this mutant. The metal-to-protein ratios in H177A and D294E were 0.22−0.26:1 and 0.33−0.35:1, respectively. The mutants with added extra metal during the reconstitution reaction or extra metal added to the assay mixture did not apparently increase metal content or enzyme activity. Therefore, His-9, His-177, and Asp-294, together with His-11 that forms the HxH motif with His-9, are likely the endogenous metal ligands. In contrast, the wild-type ACMSD and both H228A and H228E mutants presented a nearly 1:1 stoichiometric amount of Co(II) ion tightly bound within the protein interior. These experiments revealed that ACMSD's metal-binding ability was not apparently reduced in the two His-228 mutants. As described earlier, substrate binding was not significantly perturbed in these two mutants either. However, H228E was nearly an inactive protein while H228A exhibited a very small k_{cat}, i.e., a few percent of the wild-type number (Table 1). Therefore, we conclude that the invariant His-228 is not a metal ligand but it plays an important role in catalysis.

Electronic Spectra. In the wild-type Co(II)-containing ACMSD, two absorption features are present at 355 and 420 nm plus a broad weak band at 550 nm. H9E did not display these absorption features (not shown). In contrast, His-228 mutants exhibited absorption bands similar to that of the wild-type enzyme (Figure 4). Clearly, His-228 has no direct contribution to the ligand-to-metal *d*−*d* transitions in ACMSD. Surprisingly, H117A also presented a similar absorption spectrum but with lower extinction coefficient constants, offset by metal concentration determined from the EPR experiments. One explanation is that His-177 is a weaker ligand relative to the other metal-binding residues. Alternatively, another histidine, such as His-228, becomes a metal ligand in the H177A mutant, but such a ligand substitution is less likely because the metal center's geometry did not change substantially in the EPR data obtained from this mutant.

DISCUSSION

ACMSD is clearly stamped with the characteristics of the amidohydrolase superfamily by the present experiments. The concept of this protein superfamily was first introduced by Holm and Sander (*27*), later elaborated by Gerlt, Babbitt, Raushel, and others (*28*−*32*). The structural landmark of this enzyme class is a catalytically essential mononuclear or binuclear metal center embedded at the active site within the confines of a $(\beta/\alpha)_8$-barrel structural fold (*27*−*30*, *33*−*35*). This enzyme group has engendered great interest because its members are playing key roles in many fundamental processes (*28*).

The sequence analysis in the current study included more divergent members of the superfamily (Figure 2), and allowed us to narrow down the possible important residues essential for the metal cofactor and catalysis to only five amino acid targets. Further experimental analyses have identified that His-9, His-177, and Asp-294 are the endogenous metal ligands in *Pf* ACMSD. His-11 is inferred to be a metal ligand as well because of the conserved HxH metal-binding motif with His-9. Therefore, the metal ion is coordinated to four protein ligands (Figure 5). On the other hand, the mutational analysis suggests that the invariant His-228 residue does not play a role as a metal ligand. Rather, His-228 is shown by the kinetic and EPR data to be a catalytic residue. Identification of an active site histidine catalyst is consistent with the general themes of the amidohydrolase superfamily and represents a significant advance in the mechanistic study of ACMSD.

The enzymatic activities of all metal ligand mutants are drastically decreased along with a significantly reduced metal content bound to the enzyme. This clearly indicates that these metal ligands not only play a role for metal ion binding but also help to maintain a proper metal center configuration for the catalytic activity. Whether some of these ligand residues play other roles in catalysis remains to be determined.

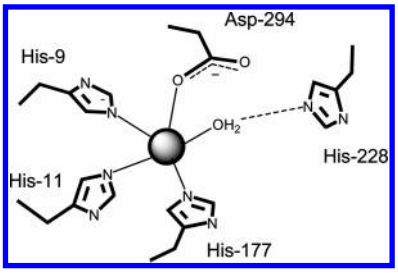

FIGURE 5: Proposed enzyme active site in ACMSD (*Pf* enzyme numbering for the amino acid residues). A divalent transition metal ion (ball) is coordinated to four endogenous protein ligands and a water molecule. His-228 was demonstrated to be an active site catalyst in the present work.

Establishing that ACMSD is a member of the amidohydrolase superfamily is a major advance for both mechanistic and evolutionary understandings of this enzyme. This assertion has now been confirmed by the crystal structure of *Pf* ACMSD recently solved in one of our laboratories (Zhang et al., to be submitted). The enzyme mechanisms of several amidohydrolases have been very well understood, such as adenosine deaminase, dihydroorotase, and urease (*28*, *33*−*39*). ACMSD may entail certain general aspects of the catalytic paradigms found in this well-studied enzyme superfamily. For example, the reaction mechanism for the elimination of ammonia in adenosine deaminase utilizes an active site histidine, which is equivalent to His-228 of *Pf* ACMSD, as a general base catalyst to abstract a proton from the water ligand to enhance its nucleophilicity (*36*, *37*). The metal-bound hydroxide then attacks the substrate to initiate the catalytic reaction. The metal center and the active site histidine catalyst in ACMSD can perhaps activate ACMS in a similar manner. Four of the metal ligands in ACMSD have been identified in the present work by a combination of bioinformatics and mutagenesis, and their critical roles in catalysis have been demonstrated with the exception of His-11. From the sequence alignment and knowledge of the characterized amidohydrolases, the fifth metal ligand in ACMSD is proposed to be a water molecule derived from solvent that forms a hydrogen bond with His-228 (Figure 5). In ACMSD, His-228 may play a role to abstract a proton from the putative water ligand and generate a metal-bound hydroxide to attack the C2−C3 double bond of the substrate. Alternatively, His-228 may function as an active site nucleophile; it directly interacts with the 2-amino group of the substrate and abstracts a proton from it, so that a substrate-based imine intermediate will be formed. This will initiate the subsequent decarboxylation process. Obviously, determining the precise role of this active site residue requires more extensive characterizations in future work.

ACMSD proteins from other organisms share a high degree of conserved residues with the *Pf* enzyme; for instance, human ACMSD not only possesses an equivalent of His-228 and the residues essential for metal cofactor but also shares an overall 40% sequence identity with *Pf* ACMSD. Therefore, the enzyme from different sources likely operates according to the same general principles with respect to a catalytic metallocofactor and an active site histidine catalyst. Thus, if the underlying decarboxylation chemistry in the nitrobenzoic acid degradation pathway can be elucidated, it may also provide insight into the enzyme of the kynurenine pathway.

Our bioinformatics study presented in Figure 2 suggests that isoorotate decarboxylase (IDCase) and ACMSD are two closely related enzymes. IDCase is an important enzyme in the thymidine salvage pathway (*40*, *41*). The overall chemical composition of isoorotate (i.e., uracil-5-carboxylate) is similar to ACMS, although the former is a phenyl ring-based compound. IDCase has previously been noticed sharing over 59% identity/similarity with ACMSD in the region covering residues 140−395 (*41*). The more comprehensive sequence analysis presented here further suggests that IDCase is also a metalloenzyme, with a conserved 3His-1Asp donor ligand set resembling the metal-binding site described for ACMSD. This enzyme shares ca. 25% overall sequence identity/similarity with ACMSD. The estimated divergent time between IDCase and ACMSD is 5.3 billion years according to an estimation formula (*42*). Despite their far evolutionary divergence, the present work suggests that the two enzymes share a high degree of similarity in their catalytic mechanisms. So far, IDCase has not been characterized at the molecular level. However, we can widen the horizon to a comparison at the genomic level as by now 16 complete ACMSD sequences and two complete IDCase sequences are annotated. Understanding how ACMSD operates sheds light on the fundamental processes that IDCase may follow.

Enzymes in the amidohydrolase superfamily catalyze hydrolysis of C−N, C−O, P−O, and C−Cl bonds, particularly in the catabolic processes of nucleotides (*28*, *31*, *32*). Notably, ACMSD and IDCase do not cleave a C−N, C−O, P−O, or C−Cl bond of the substrate. The nitrogen atoms of the substrates are retained unchanged from the decarboxylation reactions catalyzed by ACMSD or IDCase. Since the metallocofactor of IDCase has not been experimentally assessed, ACMSD is therefore the first characterized member of the amidohydrolase superfamily that catalyzes the cleavage of a C−C bond. We propose that ACMSD, together with the enzyme IDCase, constitutes an entirely new subset of decarboxylases in the amidohydrolase protein superfamily.

ACKNOWLEDGMENT

The authors thank Antoinette L. Walker for technical assistance. Shiquita L. Vaughn is acknowledged for participation in the mutant preparations under the support of the REO training program. We are indebted to Dr. Lisa Kinch for critical reading of the manuscript.

REFERENCES

1. Li, T., Walker, A. L., Iwaki, H., Hasegawa, Y., and Liu, A. (2005) Kinetic and spectroscopic characterization of ACMSD from *Pseudomonas fluorescens* reveals a pentacoordinate mononuclear metallocofactor, *J. Am. Chem. Soc. 127*, 12282−12290.
2. Schwarcz, R., Whetsell, W. O., Jr., and Mangano, R. M. (1983) Quinolinic acid: an endogenous metabolite that produces axon-sparing lesions in rat brain, *Science 219*, 316−318.
3. Stone, T. W., and Darlington, L. G. (2002) Endogenous kynurenines as targets for drug discovery and development, *Nat. Rev. Drug Discov. 1*, 609−620.
4. Stone, T. W., Mackay, G. M., Forrest, C. M., Clark, C. J., and Darlington, L. G. (2003) Tryptophan metabolites and brain disorders, *Clin. Chem. Lab. Med. 41*, 852−859.
5. Kurnasov, O., Goral, V., Colabroy, K., Gerdes, S., Anantha, S., Osterman, A., and Begley, T. P. (2003) NAD biosynthesis: identification of the tryptophan to quinolinate pathway in bacteria, *Chem. Biol. 10*, 1195−1204.
6. Schwarcz, R. (2004) The kynurenine pathway of tryptophan degradation as a drug target, *Curr. Opin. Pharmacol. 4*, 12−17.

7. Egashira, Y., Kouhashi, H., Ohta, T., and Sanada, H. (1996) Purification and properties of α-amino-β-carboxymuconate-ε-semialdehyde decarboxylase (ACMSD), key enzyme of niacin synthesis from tryptophan, from hog kidney, *J. Nutr. Sci. Vitaminol. 42*, 173−183.
8. Bender, D. A., Njagi, E. N., and Danielian, P. S. (1990) Tryptophan metabolism in vitamin B6-deficient mice, *Br. J. Nutr. 63*, 27−36.
9. Mehler, A. H. (1964) Nicotinic acid biosynthesis: control by an enzyme that competes with a spontaneous reaction, *Science 145*, 817−819.
10. Egashira, Y., Sato, M., Tanabe, A., Saito, K., Fujigaki, S., and Sanada, H. (2003) Dietary linoleic acid suppresses gene expression of rat liver α-amino-β-carboxymuconate-ε-semialdehyde decarboxylase (ACMSD) and increases quinolinic acid in serum, *Adv. Exp. Med. Biol. 527*, 671−674.
11. May, E. L., and Mehler, A. H. (1956) Studies with carboxyl-labeled 3-hydroxyanthranilic and picolinic acids in vivo and in vitro, *J. Biol. Chem. 223*, 449−455.
12. Mehler, A. H. (1956) Formation of picolinic and quinolinic acids following enzymatic oxidation of 3-hydroxyanthranilic acid, *J. Biol. Chem. 218*, 241−254.
13. Nishizuka, Y., Ichiyama, A., and Hayaishi, O. (1970) Metabolism of the benzene ring of tryptophan (mammals), *Methods Enzymol. 17*, 463−466.
14. Fukuoka, S., Ishiguro, K., Yanagihara, K., Tanabe, A., Egashira, Y., Sanada, H., and Shibata, K. (2002) Identification and expression of a cDNA encoding human α-amino-β-carboxymuconate-ε-semialdehyde decarboxylase (ACMSD). A key enzyme for the tryptophan-niacine pathway and "quinolinate hypothesis", *J. Biol. Chem. 277*, 35162−35167.
15. Tanabe, A., Egashira, Y., Fukuoka, S., Shibata, K., and Sanada, H. (2002) Purification and molecular cloning of rat 2-amino-3-carboxymuconate-6-semialdehyde decarboxylase, *Biochem. J. 361*, 567−575.
16. Muraki, T., Taki, M., Hasegawa, Y., Iwaki, H., and Lau, P. C. (2003) Prokaryotic homologs of the eukaryotic 3-hydroxyanthranilate 3,4-dioxygenase and 2-amino-3-carboxymuconate-6-semialdehyde decarboxylase in the 2-nitrobenzoate degradation pathway of *Pseudomonas fluorescens* strain KU-7, *Appl. Environ. Microbiol. 69*, 1564−1572.
17. Horton, R. M. (1995) PCR-mediated recombination and mutagenesis. SOEing together tailor-made genes, *Mol. Biotechnol. 3*, 93−99.
18. Koontz, W. A., and Shiman, R. (1976) Beef kidney 3-hydroxyanthranilic acid oxygenase. Purification, characterization, and analysis of the assay, *J. Biol. Chem. 251*, 368−377.
19. Marchler-Bauer, A., Anderson, J. B., DeWeese-Scott, C., Fedorova, N. D., Geer, L. Y., He, S., Hurwitz, D. I., Jackson, J. D., Jacobs, A. R., Lanczycki, C. J., Liebert, C. A., Liu, C., Madej, T., Marchler, G. H., Mazumder, R., Nikolskaya, A. N., Panchenko, A. R., Rao, B. S., Shoemaker, B. A., Simonyan, V., Song, J. S., Thiessen, P. A., Vasudevan, S., Wang, Y., Yamashita, R. A., Yin, J. J., and Bryant, S. H. (2003) CDD: a curated Entrez database of conserved domain alignments, *Nucleic Acids Res. 31*, 383−387.
20. Bateman, A., Coin, L., Durbin, R., Finn, R. D., Hollich, V., Griffiths-Jones, S., Khanna, A., Marshall, M., Moxon, S., Sonnhammer, E. L., Studholme, D. J., Yeats, C., and Eddy, S. R. (2004) The Pfam protein families database, *Nucleic Acids Res. 32*, D138−D141.
21. Altschul, S. F., Madden, T. L., Schaffer, A. A., Zhang, J., Zhang, Z., Miller, W., and Lipman, D. J. (1997) Gapped BLAST and PSI-BLAST: a new generation of protein database search programs, *Nucleic Acids Res. 25*, 3389−3402.
22. Pei, J., Sadreyev, R., and Grishin, N. V. (2003) PCMA: fast and accurate multiple sequence alignment based on profile consistency, *Bioinformatics 19*, 427−428.
23. McGuffin, L. J., Bryson, K., and Jones, D. T. (2000) The PSIPRED protein structure prediction server, *Bioinformatics 16*, 404−405.
24. Fukuwatari, T., Ohsaki, S., Fukuoka, S.-i., Sasaki, R., and Shibata, K. (2004) Phthalate esters enhance quinolinate production by inhibiting α-amino-β-carboxymuconate-ε-semialdehyde decarboxylase (ACMSD), a key enzyme of the tryptophan pathway, *Toxicol. Sci. 81*, 302−308.
25. Mehler, A. H., Mc, D. E., and Hundley, J. M. (1958) Changes in the enzymatic composition of liver. I. Increase of picolinic carboxylase in diabetes, *J. Biol. Chem. 232*, 323−330.
26. Tatusov, R. L., Fedorova, N. D., Jackson, J. D., Jacobs, A. R., Kiryutin, B., Koonin, E. V., Krylov, D. M., Mazumder, R., Mekhedov, S. L., Nikolskaya, A. N., Rao, B. S., Smirnov, S., Sverdlov, A. V., Vasudevan, S., Wolf, Y. I., Yin, J. J., and Natale, D. A. (2003) The COG database: an updated version includes eukaryotes, *BMC Bioinformatics 4*, 41.
27. Holm, L., and Sander, C. (1997) An evolutionary treasure: unification of a broad set of amidohydrolases related to urease, *Proteins 28*, 72−82.
28. Seibert, C. M., and Raushel, F. M. (2005) Structural and catalytic diversity within the amidohydrolase superfamily, *Biochemistry 44*, 6383−6391.
29. Gerlt, J. A., and Babbitt, P. C. (2001) Divergent evolution of enzymatic function: mechanistically diverse superfamilies and functionally distinct suprafamilies, *Annu. Rev. Biochem. 70*, 209−246.
30. Wackett, L. P. (2004) Evolution of enzymes for the metabolism of new chemical inputs into the environment, *J. Biol. Chem. 279*, 41259−41262.
31. Gerlt, J. A., and Raushel, F. M. (2003) Evolution of function in (beta/alpha)8-barrel enzymes, *Curr. Opin. Chem. Biol. 7*, 252−264.
32. Sterner, R., and Hocker, B. (2005) Catalytic versatility, stability, and evolution of the (beta/alpha)8-barrel enzyme fold, *Chem. Rev. 105*, 4038−4055.
33. Porter, T. N., Li, Y., and Raushel, F. M. (2004) Mechanism of the dihydroorotase reaction, *Biochemistry 43*, 16285−16292.
34. Hausinger, R. P. (2000) Kinetic and structural characterization of urease active site variants, *Biochemistry 39*, 8575−8584.
35. Thoden, J. B., Phillips, G. N., Jr., Neal, T. M., Raushel, F. M., and Holden, H. M. (2001) Molecular structure of dihydroorotase: a paradigm for catalysis through the use of a binuclear metal center, *Biochemistry 40*, 6989−6997.
36. Wang, Z., and Quiocho, F. A. (1998) Complexes of adenosine deaminase with two potent inhibitors: X-ray structures in four independent molecules at pH of maximum activity, *Biochemistry 37*, 8314−8324.
37. Wilson, D. K., Rudolph, F. B., and Quiocho, F. A. (1991) Atomic structure of adenosine deaminase complexed with a transition-state analog: understanding catalysis and immunodeficiency mutations, *Science 252*, 1278−1284.
38. Wilson, D. K., and Quiocho, F. A. (1994) Crystallographic observation of a trapped tetrahedral intermediate in a metalloenzyme, *Nat. Struct. Biol. 1*, 691−694.
39. Jabri, E., Carr, M. B., Hausinger, R. P., and Karplus, P. A. (1995) The crystal structure of urease from *Klebsiella aerogenes*, *Science 268*, 998−1004.
40. Palmatier, R. D., McCroskey, R. P., and Abbott, M. T. (1970) The enzymatic conversion of uracil 5-carboxylic acid to uracil and carbon dioxide, *J. Biol. Chem. 245*, 6706−6710.
41. Smiley, J. A., Kundracik, M., Landfried, D. A., Barnes, V. R., Sr., and Axhemi, A. A. (2005) Genes of the thymidine salvage pathway: Thymine-7-hydroxylase from a *Rhodotorula glutinis* cDNA library and iso-orotate decarboxylase from *Neurospora crassa*, *Biochim. Biophys. Acta 1723*, 256−264.
42. Feng, D.-F., Cho, G., and Doolittle, R. F. (1997) Determining divergence times with a protein clock: Update and reevaluation, *Proc. Natl. Acad. Sci. U.S.A. 94*, 13028−13033.
43. Ireton, G. C., McDermott, G., Black, M. E., and Stoddard, B. L. (2002) The structure of *Escherichia coli* cytosine deaminase, *J. Mol. Biol. 315*, 687−697.
44. Liaw, S. H., Chen, S. J., Ko, T. P., Hsu, C. S., Chen, C. J., Wang, A. H., and Tsai, Y. C. (2003) Crystal structure of D-aminoacylase from *Alcaligenes faecalis* DA1. A novel subset of amidohydrolases and insights into the enzyme mechanism, *J. Biol. Chem. 278*, 4957−4962.
45. Nitanai, Y., Satow, Y., Adachi, H., and Tsujimoto, M. (2002) Crystal structure of human renal dipeptidase involved in beta-lactam hydrolysis, *J. Mol. Biol. 321*, 177−184.
46. Pearson, M. A., Michel, L. O., Hausinger, R. P., and Karplus, P. A. (1997) Structures of Cys319 variants and acetohydroxamate-inhibited *Klebsiella aerogenes* urease, *Biochemistry 36*, 8164−8172.
47. Thoden, J. B., Marti-Arbona, R., Raushel, F. M., and Holden, H. M. (2003) High-resolution X-ray structure of isoaspartyl dipeptidase from *Escherichia coli*, *Biochemistry 42*, 4874−4882.
48. Benning, M. M., Kuo, J. M., Raushel, F. M., and Holden, H. M. (1995) Three-dimensional structure of the binuclear metal center of phosphotriesterase, *Biochemistry 34*, 7973−7978.

BI060108C